Gas-Phase Spectroscopy of the Unstable Acetonitrile *N*-Oxide Molecule, CH_3CNO

Tibor Pasinszki*,† and Nicholas P. C. Westwood*,‡

Department of Inorganic Chemistry, Budapest University of Technology and Economics, H-1521 Budapest, Gellért tér 4, Hungary, and Guelph-Waterloo Centre for Graduate Work in Chemistry, Department of Chemistry and Biochemistry, University of Guelph, Guelph, Ontario, Canada N1G 2W1

Received: August 7, 2000; In Final Form: December 8, 2000

The unstable acetonitrile *N*-oxide molecule, CH_3CNO, has been thermolytically generated in very high yield in the gas phase from its stable ring dimer, dimethylfuroxan, and studied by ultraviolet photoelectron spectroscopy, photoionization mass spectroscopy, and mid-infrared spectroscopy. The individual spectroscopies provide a detailed investigation into the vibrational and electronic character of the molecule, and are supported by both conventional ab initio calculations and density functional theory. The ground-state structure is also investigated by theory at the B3-LYP, MP*n* ($n = 2-4$), QCISD, and QCISD(T) levels with medium to large basis sets, and illustrates the need for a precise description of electron correlation. Given that both isomerization and dimerization are feasible loss processes for this unstable molecule, the relative stability of CH_3CNO with respect to the known cyanate (CH_3OCN), isocyanate (CH_3NCO), and fulminate (CH_3ONC) isomers and the mechanism of the dimerization processes were studied with density functional theory.

Introduction

Several open-chain isomers of simple pseudohalide molecules containing a "CNO" group can be drawn, some of which are known experimentally. The methyl derivatives represent the only example of small pseudohalides where the three lowest energy isomers (isocyanate (−NCO), cyanate (−OCN), and nitrile oxide (−CNO) in order of decreasing thermodynamic stability) are known and can be cleanly generated in the gas phase. CH_3NCO is a liquid at room temperature (boiling point, 44−46 °C),[1] the generation and gas-phase spectroscopy of the semistable CH_3OCN molecule was recently reported,[2,3] and a gas-phase investigation of pure CH_3CNO is discussed in the present work. A fourth open-chain isomer (excluding the unreasonable valence structures −NOC and −CON) is the much higher energy fulminate, CH_3ONC, observed by low-temperature infrared (IR) spectroscopy.[4]

Substituted nitrile oxides, X−C≡N→O, the archetypal 1,3-dipolarophiles, have proven to be useful reagents in synthetic organic chemistry. Because of their high reactivity and propensity to dimerize, they are not isolated, but rather are generated in situ for various dipolar cycloaddition reactions including formation of substituted heterocycles such as 2-isoxazolines, isoxazoles, 1,3,4-dioxazoles, 1,2,4-oxadiazoles,[5] and many important biologically active compounds.[6] More recently, the smaller derivatives (X = Br−,[7,8] Cl−,[9,10] NC−,[11] and ONC−[12]) have been generated as unstable molecules in the gas phase. Of interest are their structures and the associated spectroscopy,[8,10,13−15] bringing into focus issues of quasi-linearity, the efficacy of quantum mechanical calculations to predict structures and barriers to linearity,[7,9,11,12,16,17] and for those species containing the relatively abundant elements C, N, O, and H possible candidacy for astrophysical observation.

In the present work we discuss the gas-phase generation and first characterization of the CH_3CNO molecule, **1**, in the gas phase by ultraviolet photoelectron (PE), photoionization mass (PIM), and mid-IR spectroscopies, and consider potential loss processes involving isomerization and/or dimerization. Relatively stable large aromatic nitrile oxides are known to isomerize to isocyanates upon heating, whereas the primary loss process of small nitrile oxides is dimerization.[5] Thus, **1** is unstable at room temperature, dimerizing within 1 min at 18 °C to the dimethylfuroxan ring, **2** (3,4-dimethyl-1,2,5-oxadiazole 2-oxide), thereby inhibiting investigation in the gas phase. It is stated, however,[18] that **1** can be stored at temperatures well below 0 °C. For solution chemistry **1** is normally generated in situ by dehydrohalogenation of acetohydroxamyl chloride (α-chloroacetaldoxime)[19] or by dehydration of nitroethane.[5] Of relevance to the present gas-phase work is the observation that **1** can be generated from its stable ring dimer, **2**, using the flash vacuum thermolysis (FVP) method (600 °C, 10^{-3} Torr).[20] Nonetheless, the IR spectrum of **1** has only been investigated in solutions of CCl_4, CS_2, and cyclohexane,[18] and matrix IR has identified **1** following photolysis of acetonitrile and $O(^3P)$ atoms.[21] The only published gas-phase spectroscopy is the microwave (MW)[22,23] and millimeter wave spectra[24] of samples obtained by the standard route of HCl elimination from α-chloroacetaldoxime.[19] The analyzed r_s structure indicates that **1** is a symmetric top (C_{3v}) with a large dipole moment (4.49 D).

Early ab initio calculations limited to the Hartree−Fock (HF) level with modest (STO-3G, 4-31G, 6-31G*) basis sets[25,26] suggested that **1** had a linear CCNO frame, in agreement with the MW results. This was fortuitous since it is now well-known that large basis sets and the inclusion of electron correlation are of crucial importance in the prediction of the structures of nitrile oxides,[7,9,11,16,17,27] In the present work ab initio calculations (including density functional theory (DFT) methods) are used to assess the effect of basis set size and electron correlation on the calculated versus MW structure of **1**, and to assist in the analysis of the PE and IR data. Since **1** and the better known isomers CH_3NCO and CH_3OCN can potentially interconvert and are of interest as model compounds for substituted R(CNO) species, comparison is made to the spectroscopy and structure

* To whom correspondence should be addressed. E-mail: pasinszki.inc@chem.bme.hu, westwood@chembio.uoguelph.ca.
† Budapest University of Technology and Economics.
‡ University of Guelph.

10.1021/jp002851z CCC: $20.00
Published on Web 02/02/2001

SCHEME 1

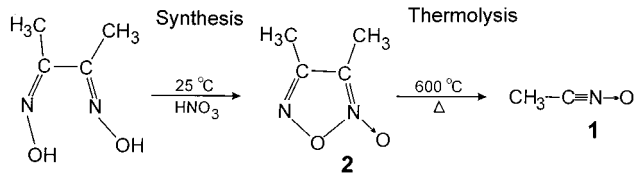

of these isomers, including DFT calculations of their bending potentials, and the unimolecular isomerization processes of **1** to the other isomers. The dominant loss process of **1**, dimerization to the ring furoxan **2**, is also considered using DFT.

Experimental Section

The specifics of the generation of **1** from the stable dimer precursor **2** are given below in the Results and Discussion. Several methods of synthesizing **2** are known. Many are multistep procedures often utilizing the oxidizing power of liquid dinitrogen tetroxide, N_2O_4. One of the simplest (and oldest) methods describes the oxidation of dimethylglyoxime with N_2O_4.[28] Since it has been noted that dichloroglyoxime can be oxidized to dichlorofuroxan using white fuming HNO_3,[29] and since the handling of liquid nitric acid, HNO_3, is easier than that of N_2O_4, we adopted and modified this latter method using concentrated HNO_3 to prepare **2** from dimethylglyoxime (Aldrich), Scheme 1.

A 40 g sample of dimethylglyoxime was added slowly (3 h), with stirring, to 300 mL of concentrated nitric acid (68% *m*/*m*) at room temperature. The evolution of brown nitrogen oxides was observed instantly, the solution turning brown. Upon completion of the addition of dimethylglyoxime, the solution was stirred for 1 h, poured onto ice, and extracted with 3 × 100 mL of dichloromethane. The extract was washed with ice water until neutral, dried over magnesium sulfate, and evaporated. A 25 mL sample of a pale green raw product was obtained, which was distilled four times through a 15 cm long Vigreux column, giving **2** as an almost colorless liquid with a boiling point of 50−52 °C at ca. 2.5 mmHg. The purity was confirmed by IR spectroscopy. The repeated distillations were of crucial importance in obtaining pure **2**, since the boiling point of the green side product (not identified in this work) was only 4 °C lower at 2.5 mmHg than that of **2**. Due to the loss of **2** during the repeated purification process, the final yield was low, ca. 30%, but this could certainly be improved using more sophisticated purification methods.

HeI (21.2 eV) PE spectra were recorded on a fast-pumping spectrometer specifically designed to study reactive and unstable species.[30,31] The resolution was ca. 45 meV during the experiments, with spectra calibrated using the known ionization potentials (IPs) of O_2 and N_2. Mass analysis of ions is achieved with a quadrupole mass analyzer (Hiden Analytical, 320 amu) mounted directly above the photoionization point. With the conventional EI source removed, ionization is provided by single-wavelength HeI or unfiltered $HL_{\alpha,\beta,\gamma}$ (10.2−12.7 eV) radiation. PE and PIMS spectra, although not done in coincidence, can be recorded within seconds of each other under identical conditions; thus, it is assumed that for a given PE spectrum the subsequent PIMS is of the same compound.

Mid-IR spectra of **1** were collected on a Nicolet 20SXC interferometer equipped with a 20 cm single-pass cell. The cell, with KBr windows, gave a spectral range down to 350 cm^{-1}. The effluent from the pyrolysis tube or sample container was pumped continuously through the cell using a rotary pump while the pressure was kept constant between 450 and 500 mTorr. The spectra were recorded at 0.5 cm^{-1} resolution.

Computational Methods

Ab initio calculations for the structure of **1** were carried out at the MP2, MP3, MP4SDQ, MP4 (=MP4SDTQ), QCISD, and QCISD(T) levels using standard basis sets, viz., 6-31G**, 6-311G(2d,2p), or cc-pVTZ (Dunning's correlation-consistent basis set; [4s,3p,2d,1f] on C, N, and O atoms, and [3s,2p,d] on H atoms). All electrons were included in the correlation energy calculations (i.e., "full"). DFT, in the form of B3-LYP (Becke's three-parameter exchange functional in combination with the Lee, Yang, and Parr correlation functional), was also used to calculate the equilibrium structure of **1**. Isomerization of **1**, the interconnecting transition states (TSs), and the dimerization mechanism were investigated at the cost-effective B3LYP/6-31G** level. Equilibrium molecular geometries were fully optimized and harmonic vibrational frequencies calculated at the minimum-energy geometries to confirm them as real points on the potential energy surface (zero imaginary frequencies). TSs were characterized by one imaginary frequency. IPs for **1** were calculated using the HAM/3[32] and the outer valence Green's function (OVGF) methods.[33] All calculations were performed with the Gaussian-92 and Gaussian-94 quantum chemistry packages[34,35] implemented on Silicon Graphics Inc. Challenge/XL and Origin 200 workstations.

Results and Discussion

Generation, Identification, and Stability of CH_3CNO, 1. For direct gas-phase generation of **1** the methods used for in situ 1,3-dipolar cycloadditions in solution[5,19] are inappropriate due to unwanted elimination products (e.g., HCl from acetohydroxamoyl chloride). An approach based on the thermolytic cycloreversion of **2**[20] offers a direct route capable of generating **1** as the sole product for spectroscopic investigation. Precedents for this approach also include our recent demonstration of the clean generation of NCCNO from its stable furoxan dimer[11] and the use of this method by other groups.[36] By attaching the thermolysis tube directly to the spectrometers, we could monitor the efficiency of the thermolytic cycloreversion, and directly observe potential intramolecular rearrangements to isomers of **1** (e.g., the isocyanate), or possible dimerization.

Thermolysis of **2** was carried out in a quartz tube (8 mm i.d.) heated along 15 cm, packed with quartz chips to improve efficiency. The FVP of **2** led to smooth formation of **1** at 600 °C. From the various spectroscopies (below) which confirmed the identity of the molecule, the direct gas-phase yield of **1** can be almost quantitative, with only trace amounts of CO, CO_2, NO, CH_3NCO, and CH_3CN as side products. Purer samples could be obtained by condensing **1** at −196 °C in a U-trap connected to the IR cell or PE spectrometer and then gradually warming, pumping off traces of side products below −20 °C. **1** had sufficient vapor pressure at −20 °C for PES and PIMS, and at −10 °C for IR investigation. After the spectra were recorded, the temperature was increased to 0 °C; only gaseous **1** was observed at this temperature, indicating that dimerization of the trapped material is slow, unlike the case of BrCNO.[7] This trapping/revaporizing result suggests that **1** could be trapped and stored at liquid N_2 temperatures, and then recovered upon warming. There was no indication of isomerization of **1** under these conditions.

Computational Investigation of the Structure of 1. Since the inclusion of electron correlation is de rigeur for calculations on simple nitrile oxides,[7,9,11,16,17,27] the geometry of **1** was

TABLE 1: Calculated Barriers to Linearity, Equilibrium Structures, Total Energies, Rotational Constants, and Dipole Moments of CH_3CNO, 1[a]

	MP2	MP3	MP4SD Q	MP4	QCISD	QCISD(T)	B3-LYP	exptl MW[22]
				Barrier to Linearity[b]				
basis set								
cc-pVTZ	0.0						0.0	
6-311G(2d,2p)	(19.3)	0.0	0.0	126.6	0.0	0.0	(0.0)	
6-31G**	(75.5)	(0.0)	(0.0)	(226.4)	(0.0)	(0.0)	(0.0)	
				Structure for the Largest Basis Set and Experimental Structure				
C−C	1.453	1.466	1.468	1.477	1.469	1.471	1.456	1.442
C−N	1.174	1.148	1.159	1.191	1.156	1.166	1.156	1.169
N−O	1.198	1.210	1.216	1.213	1.221	1.221	1.210	1.217
C−H	1.085	1.084	1.086	1.087	1.086	1.088	1.091	no data for
C−H″				1.089				H params
CCN	180.0	180.0	180.0	154.5	180.0	180.0	180.0	180.0
CNO	180.0	180.0	180.0	172.7	180.0	180.0	180.0	180.0
HCC	110.6	110.2	110.3	110.4	110.2	110.3	110.7	
H″CC				110.5				
total energy	−207.588165	−207.520477	−207.536622	−207.582668	−207.536014	−207.570355	−207.981613	
A[c]	161.9197	161.4988	161.1145	121.6789	160.9994	160.5556	160.5408	
B	3.9180	3.9312	3.8926	3.9500	3.8890	3.8608	3.9266	3.914796
C	3.9180	3.9312	3.8926	3.9196	3.8890	3.8608	3.9266	
μ[d]	5.276	5.406	5.460	5.002	5.482	5.436	4.271	4.49

[a] Bond angles in deg, bond lengths in Å, total energies in au. For the structures, the cc-pVTZ basis set was used at the B3-LYP and MP2 levels and the 6-311G(2d,2p) basis set was used at the MP3, MP4, and QCI levels. All of the electrons were included in the correlation energy calculations ("full"). [b] Barriers to linear CCNO frame in cm^{-1}. Values in parentheses refer to barriers obtained with smaller basis sets. [c] Rotational constants in GHz. [d] Dipole moments in D.

calculated at various levels of post-HF theory, with increasing basis set size from 6-31G** through 6-311G(2d,2p) to cc-pVTZ to study basis set effects.

The calculated equilibrium geometry of **1** is shown in Table 1, and concurs (but see below) with the experimental r_s geometry of the heavy atoms obtained from the MW data,[22] which suggest a symmetric-top molecule with a linear CCNO frame. From the *l*-type doubling constant a value of 150(50) cm^{-1} was obtained for the lowest frequency deformation, insufficiently low enough to indicate quasi-linear behavior,[24] but suggesting that, as with other simple nitrile oxides, difficulties with calculated structures might be expected. Indeed, the calculated structures fall into the familiar pattern,[7,9,11] with respect to both the size of the basis set and the level of electron correlation. With the smallest basis set (6-31G**) the MP3, MP4SDQ, QCISD, QCISD(T), and B3-LYP levels predict a linear CCNO frame, whereas MP2 and MP4SDTQ predict a bent molecule. Increases in basis set size decrease the barrier to linearity, with the calculated structure becoming linear at MP2/cc-pVTZ. Correspondingly, the C≡N bond, which is strongly correlated to the CCN angle, is shortest at linearity, e.g., with MP2, 1.193 Å (6-31G**) → 1.181 Å (6-311G(2d,2p) → 1.174 Å (cc-pVTZ). Resource limitations precluded further increases in basis set size at the MP4SDTQ level, where **1** is still bent, but we expect the same trend toward linearity to hold.

The strong electron correlation effects on calculated properties noted previously (BrCNO,[7] ClCNO,[9] and HCNO[27]) are demonstrated by an oscillatory behavior in the MP*n* expansion series (MP1=HF, MP2, MP3, MP4), for example, the C≡N bond length using the 6-311G(2d,2p) basis set (1.123, 1.181, 1.148, and 1.191 Å, respectively), barrier height (0, 19.3, 0, and 126.6 cm^{-1}, respectively), and total energy (Table 1). The other effect is that triple excitations markedly lengthen the C≡N bond length, tending to bend the structure; compare MP4SDQ with MP4SDTQ and QCISD with QCISD(T). MP4SDTQ clearly overestimates the C−C and C≡N bond lengths and barrier height, in accord with the known fact that the method exaggerates triple contributions to the correlation energy.[37] By including a better description of triple excitations at the QCISD-(T) level,[38] the linear geometry of the molecule is reproduced and the calculated geometry is in better agreement with the experimental structure. Clearly, the electron-rich nature of nitrile oxides poses a serious computational challenge due to large and sensitive electron correlation effects, and demands the use of extra large basis sets and very high levels of theory when accurate structural and spectroscopic properties are calculated. This has been demonstrated recently in calculations for the structure of HCNO[27] and in calculating energy levels in the region of the barrier for BrCNO[16] and ClCNO.[17]

We note here that if very high level conventional ab initio calculations are not feasible, DFT (e.g., using B3-LYP) can provide a reliable cost-effective alternative, giving, for nitrile oxides, reasonable results for structures (Table 1) and good agreement with vibrational frequencies. For this reason we have used the B3-LYP method in calculations of the related isomers and their interconversions, and for evaluating the dimerization process (below).

The known structural differences between **1** and the CH_3-NCO and CH_3OCN isomers suggest different electronic structures and chemical reactivities. To highlight these before discussing the spectroscopy, we have calculated the (B3-LYP/cc-pVTZ) structures of these two other isomers (where MW structures are also known[39,40]) and compared the potentials of their lowest frequency deformations with that of **1**. Figure 1 demonstrates that CH_3OCN has a steep harmonic well, which becomes progressively more anharmonic in CH_3NCO and CH_3-CNO. The fitted potentials are as follows:

$$CH_3OCN: V(cm^{-1}) = 7830.60 + 22.751\rho - 6.360\rho^2 + 0.064\rho^3$$

$$CH_3NCO: V(cm^{-1}) = 595.95 + 4.646\rho - 1.191\rho^2 + 0.014\rho^3 + 0.00010\rho^4$$

$$CH_3CNO: V(cm^{-1}) = 0.581\rho^2 + 0.00016\rho^4$$

where ρ is the deviation from 180° at the central atom. What

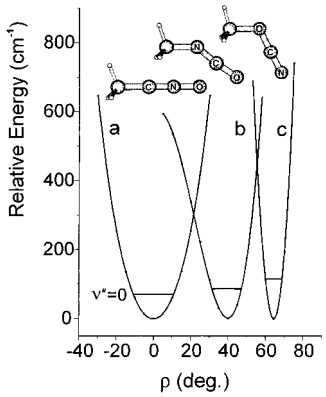

Figure 1. Calculated (B3-LYP/cc-pVTZ) potentials (constructed by optimizing every 5°) of the lowest frequency deformations in (a) CH_3CNO, (b) CH_3NCO, and (c) CH_3OCN.

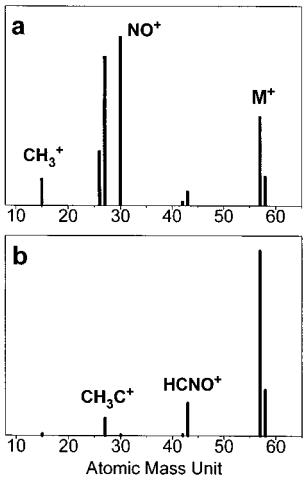

Figure 2. (a) HeI and (b) $HL_{\alpha,\beta,\gamma}$ photoionization mass spectra of CH_3CNO.

emerges is that CH_3OCN is strongly bent and rigid (small amplitude deformation), CH_3CNO is linear and floppy (large amplitude deformation at the central carbon atom), and CH_3NCO is in between, its frame being less bent, but more flexible than that of CH_3OCN. These pronounced structural differences are reflected in the spectroscopy.

Photoionization Mass Spectroscopy. The HeI and $HL_{\alpha,\beta,\gamma}$ PIMS spectra of **1** (Figure 2) are relatively simple, confirm its identification, and clearly distinguish it from the cyanate and isocyanate isomers (see Figure 2 in ref 2), the cracking patterns being quite different. The base peaks in the HeI PIMS of **1**, CH_3NCO, and CH_3OCN are NO^+, CO^+, and CH_3^+, respectively. NO^+ is observed only with **1**, quite typical for nitrile oxides.[7,11,12] CO^+ is not observed in the PIMS of **1**, and is relatively small for CH_3OCN. The CH_3^+ fragment, with a strong relative intensity in the $HL_{\alpha,\beta,\gamma}$ PIMS of CH_3OCN, is not observed in the corresponding PIMS of CH_3NCO and is negligible for **1**.

The three strongest peaks in the HeI PIMS of **1**, the molecular ion (M^+), and NO^+ and XC^+ ($X = -CH_3$) fragments are also seen in the spectra of other XCNO molecules ($X = Br-$,[7] NC−,[11] ONC−[12]). Their relative intensities are different, however, as the NO^+ peak dominates the HeI spectra of BrCNO, NCCNO, and ONCCNO, with only a small-intensity XC^+ fragment. For **1**, the relative intensity (compared to that of M^+) of NO^+ has strongly diminished while that of XC^+ has increased, showing that the probability of neutral NO loss from the excited M^+ ion increases by replacing the electronegative halide ($X = Br-$) or pseudohalide ($X =$ ONC−, NC−) group by electropositive $-CH_3$. Other fragments also observed for **1** are $(M + 1)^+$, $HCNO^+$, CNO^+, CH_2C^+, and CH_3^+. The $(M + 1)^+$ fragment also seen with the CH_3NCO and CH_3OCN isomers[2] may result from secondary ion reactions in the quadrupole. This may also explain the observation of $HCNO^+$ and CNO^+ fragment pairs. Fragmentation is usually reduced in the $HL_{\alpha,\beta,\gamma}$ PIMS due to the lower energy light source and is reflected in the strong increase in the parent ion signal and negligible NO^+ and CH_3^+ fragments.

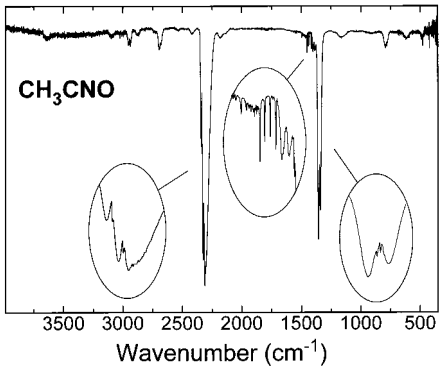

Figure 3. Gas-phase mid-infrared spectrum of CH_3CNO at ca. 450 mTorr and 0.5 cm^{-1} resolution. Insets show details of the ν_2, ν_7 and ν_3, and ν_4 bands.

Infrared Spectroscopy. The gas-phase IR spectrum of **1** is shown in Figure 3 with the vibrational frequencies of the fundamentals provided in Table 2 together with the calculated (B3-LYP/cc-pVTZ and QCISD/6-31G**), unscaled, vibrational frequencies and intensities. For comparison, Table 2 also includes the data on this molecule from the only other known (solution[18] and matrix[21]) IR work. The observed spectrum confirms the identity of **1**, the absence of the precursor/dimer molecule **2**, which has its strongest band at 1614 cm^{-1},[41] and that there is no evidence for the CH_3OCN and CH_3NCO isomers. **1** is the sole species in the gas phase, with almost all bands (weak and strong) being assignable to either fundamentals or overtone/combination bands.

The 15 normal modes of **1** transform in C_{3v} symmetry as $5A_1 + 5E$, and all but the lowest frequency bending mode (ν_{10}), are observed in this work. For such a symmetric top, parallel-type bands of a_1 symmetry ($A_1 \leftarrow A_1$ transition) should exhibit P, Q, and R structure arising from overlapping $K = 0, 1, 2, ...$ subbands. However, in a case such as **1** where I_A/I_B is small (i.e., $A \gg B$), the Q branch is predicted to have a low intensity.[42] Perpendicular transitions ($E \leftarrow A_1$) in a symmetric top can lead to the classic, and often prominent, ^rQ and ^pQ subbands (due to different K values) with a separation given by $2[A(1 - \zeta_i) - B]$, where ζ_i is the Coriolis coupling constant. Both types of bands are observed, the subbands in the perpendicular transitions (in those cases where $\zeta_i \approx 0$) being clearly resolved even at 0.5 cm^{-1} resolution, and four of the five parallel transitions exhibiting unresolved P and R envelopes with a separation of band maxima of ca. 15−17 cm^{-1}.

In the CH stretching region near 3000 cm^{-1}, the most prominent band exhibiting PR structure is centered at 2943 cm^{-1} and is assigned to ν_1, the symmetric CH_3 stretch of a_1 symmetry. The antisymmetric CH_3 stretch, ν_6(e), to higher wavenumber, is much weaker, as predicted by the calculations. Such an $E \leftarrow A_1$ perpendicular transition has its intensity distributed into the ^rQ and ^pQ subbands, which show evidence of intensity alternation (..., strong, weak, weak, strong, ...) due to nuclear spin statistics, despite the poor signal/noise ratio. The observed

TABLE 2: Experimental[a] and Calculated[b] Vibrational Frequencies (cm^{-1}) of the Fundamental Vibrations of CH_3CNO

experimental			B3-LYP/cc-pVTZ		QCISD/6- 31G**		assignment and description
gas	soln[c]	matrix[d]	freq (sym)	intens[e]	freq (sym)	intens[e]	
3022.5[f] vvw	2967		3089 (E)	4.5	3213 (E)	5.2	ν_6 CH as str
2950 R, 2935 P } w	2924		3028 (A_1)	17.7	3125 (A_1)	17.5	ν_1 CH sym str
2311[g] vs	2315	2309	2455 (A_1)	429.6	2493 (A_1)	324.5	ν_2 CNO as str
1453.2[h] vw	1441		1478 (E)	8.7	1540 (E)	7.3	ν_7 CH_3 as def
1401 R, 1386 P } vw	1381	1381	1428 (A_1)	21.2	1478 (A_1)	0.1	ν_3 CH_3 sym def
1356 R, 1348.9 Q, 1346.3 Q, 1340 P } i_s	1319	1332	1389 (A_1)	195.2	1379 (A_1)	140.2	ν_4 CNO sym str
1034 vvw (see the text re the band at 1162)	1177		1051 (E)	1.0	1083 (E)	0.5	ν_8 CH_3 rock
791 R, 788.1 Q, 781.9 Q, 777 P } i_w	778	780	795 (A_1)	20.4	799 (A_1)	26.1	ν_5TC−C str
477.3 vw[j]	478		510 (E)	4.0	493 (E)	6.8	ν_9 CNO bend
(150 (50))[k]	297		137 (E)	1.4	112 (E)	0.9	ν_{10} CCN bend

[a] Band positions (gas) taken from the maxima or sharp features of the IR bands. [b] Unscaled harmonic frequencies. [c] From ref 18. [d] From ref 21. [e] In km/mol. [f] Sharp $^rQ/^pQ$ subbands (cm^{-1}) at 3022.5 (most intense), 3012.8, 3003.9, 2993.8(s), 2984.3, 2973.9, 2965.1(s), and 2936 (s) (overlapping ν_1) (see the text). [g] Strongest peak of a complex band (see the text). [h] Sharp $^rQ/^pQ$ subbands (cm^{-1}) at 1453.2 (most intense), 1442.1, 1429.3, 1416.1(s), 1403 and 1388 (overlapping ν_3), and 1373.8 (overlapping ν_4) (see the text). [i] See the text regarding possible difference bands. [j] Central spike. [k] From ref 24 obtained from the microwave spectrum, ref 22.

subband spacings are about 9 cm^{-1}, the line positions being given as a footnote to Table 2. We cannot unambiguously identify the band origin; the center of the four strongest observed subbands is at about 2980 cm^{-1}, although the most intense subband at 3022.5 cm^{-1} is listed in the table as the nominal band center.

The two most prominent bands in the spectrum, characteristic of all nitrile oxides, are centered at 2311 and 1348 cm^{-1} corresponding to the antisymmetric (ν_2) and symmetric (ν_4) CNO stretches, both of a_1 symmetry. Their relative intensities are well predicted by the ab initio calculations. The symmetric stretch shows PR structure with what looks like two Q branches (labeled as such in Table 2), although one of these may arise from a difference band of the type $\nu_4 + \nu_{10} - \nu_{10}$. The antisymmetric stretch shows a complicated rotational profile consistent with the concurrent excitation of low-frequency bending modes. The value of 2311 cm^{-1} is assigned to the most intense feature, although Q branches at 2305, 2318, and 2333 cm^{-1} are observed. Such hot band structure was observed previously on the antisymmetric CNO stretches of BrCNO,[7] ClCNO,[9] NCCNO,[11] and ONCCNO.[12,13]

To the high wavenumber side of the symmetric stretch centered at 1348 cm^{-1} are two additional weak bands with quite different rotational profiles (see the insets of Figure 3), predicted by the ab initio calculations to correspond to the antisymmetric ν_7(e) and symmetric $\nu_3(a_1)$ CH_3 deformations. These are identified, respectively, at 1453.2 cm^{-1} (most intense subband of the well-spaced ^rQ and ^pQ subbands of an $E \leftarrow A_1$ perpendicular transition) and 1394 cm^{-1} (center of the PR structure), mimicking in profile the close e and a_1 pair (ν_6 and ν_1) in the CH_3 stretching region. The degenerate mode exhibits the expected intensity alternation due to nuclear spin statistics; the positions of these subbands, with an average spacing of about 13 cm^{-1}, are given as a footnote to Table 2. This spacing is somewhat higher than that observed for ν_6 (ca. 9 cm^{-1}), but understandable in terms of the possible allowed values (between +1 and −1) of ζ_i. In the absence of the Coriolis force ($\zeta_i = 0$), the calculated rotational constants (Table 1) predict a value of ca. 10.5 cm^{-1} for the subband separation. A curious feature (possibly arising from an A−E Coriolis interaction and a resulting intensity perturbation) is the sudden decrease of the subband intensity to the high-wavenumber side, although weaker structure extending up to ca. 1570 cm^{-1} can be observed. As with ν_6 this makes location of the ν_7 band center problematic, and although we list the strongest subband peak at 1453.2 cm^{-1} in Table 2, the actual band center could be higher. A likely combination band, $\nu_4 + \nu_{10}$ of E symmetry, would also appear in this region, potentially leading to a Fermi resonance.

Below 1200 cm^{-1} are four weak but distinct bands, two of which, on the basis of their band structure, can be assigned to the fundamentals $\nu_5(a_1)$ (785 cm^{-1}) and ν_9(e) (477 cm^{-1}), respectively, the CC stretch and the CNO bend. The positions of these normal modes are in good agreement with the calculated frequencies, as are the intensities, with the more intense ν_5 showing PR structure and two central Q branches again possibly resulting from difference bands. The perpendicular band ν_9 exhibits K structure, albeit not as clear as in ν_6 and ν_7, with extra "spiked" intensity in the center of the band, suggesting that $\zeta \approx 1$, and/or $A' \neq A''$ and $B' \neq B''$. The remaining fundamental in our range, the CH_3 rock ν_8(e), is more problematic. On the basis of the solution work,[18] which places ν_8 at 1177 cm^{-1}, we should assign the observed band at 1162 cm^{-1} to this mode. However, we note (Table 2) that the calculated intensity for this band is exceedingly low, 20−50 times less than for the adjacent ν_5, and the position calculated by both computational methods is 110−80 cm^{-1} lower, the only time that the (unscaled) calculations give a lower value than experiment. Perhaps more convincing is the fact that the comparable CH_3 rock in the similar molecule CH_3CN[43] is located at 1041 cm^{-1}. There is a very, very weak band at 1034 cm^{-1} in the spectrum, which we believe is a more likely contender for ν_8. The lowest bending mode ν_{10} is not observed in this work, having been estimated[24] from the *l*-type doubling constant *q* obtained in the microwave spectrum[22] to be 150(50) cm^{-1}, although the solution work places this band at 297 cm^{-1} (see also below).

A comparison of the present gas-phase data with the solution[18] and matrix work[21] shows good correspondence (apart from ν_8), the main discrepancies arising from the precise location of the degenerate modes ν_6 and ν_7, where, as noted above, the position

TABLE 3: Experimental Vibrational Frequencies (cm^{-1}) of the Very Weak Bands in the IR Spectrum of CH_3CNO Assigned to Overtone, Combination, and Other Bands

(exptl (gas)	tentative assignment	qualifier
3634	$\nu_2 + \nu_4$ (A_1)	? depends on band center of ν_2[a]
3096	$\nu_2 + \nu_5$ (A_1)	
2880 R, 2865 P	$\nu_3 + \nu_7$ (E)	? depends on band center of ν_7[b]; ? but not predicted to have PR structure
2743 R, 2727 P	$\nu_3 + \nu_4$ (A_1)	
2694 R, 2685 Q, 2682 Q, 2679 P	$2\nu_4$ (A_1)	
2533	$2\nu_8 + \nu_9$ (A_1, E)	? depends on band center of ν_8[c]
2422 R, 2415 Q	$\nu_3 + \nu_8$ (E)	? depends on band center of ν_8[c]; ? but not predicted to have RQ structure
2179	$\nu_3 + \nu_5$ (A_1) or $\nu_2 - \nu_{10}$ (E)	predicts ν_{10} at ca. 132 cm^{-1}
2057 R, 2042 P	$2\nu_8$ (A_1, E)	? depends on band center of ν_8[c]
1788	?	
1162	$\nu_8 + \nu_{10}$ (A_1, E)	? depends on band center of ν_8[c]; predicts ν_{10} at ca. 128 cm^{-1}
910	$\nu_5 + \nu_{10}$ (E)	predicts ν_{10} at ca. 125 cm^{-1}
615	$\nu_9 + \nu_{10}$ (A_1, E)	predicts ν_{10} at ca. 135 cm^{-1}

[a] Hot bands on ν_2 (see the text) preclude a precise determination of the band center. [b] A perpendicular-type band structure precludes a precise determination of the band center. [c] Depends on precise location of the band center for the very, very, weak ν_8 band.

of the band centers is uncertain. In Table 2 we have picked the most intense ^rQ or ^pQ subbands as the band identifiers, although in both modes weaker subbands march to lower and higher energy. The unscaled harmonic calculations do a reasonable job for the band positions and intensities, and directed us to considering an alternative location for ν_8. Overall the B3-LYP method performs better than QCISD, although appropriate scaling factors could diminish this difference. The CN and NO stretches, which we have labeled as ν_{as}(CNO) and ν_s(CNO), respectively, do show large calculated deviations, evidence for strong coupling in these modes.

Table 3 provides a summary of the remaining weak features in the spectrum, which are assigned to either overtones or combination bands or are unknown. The point should be made that these bands seem to track in intensity with the fundamentals, and so we have some confidence in assigning them to bands of **1**; some exhibit a ΔPR of ca. 15−17 cm^{-1} consistent with the fundamentals of **1**. Several of the combination bands are assigned in Table 3 with no commentary. Others, which are perhaps more insecure, have associated comments. These arise, in the main, because of the uncertainty in the band centers of ν_2 and ν_7 and the predilection for placing ν_8 at 1034 cm^{-1} rather than the more obvious 1162 cm^{-1} position (vide supra), as well as the uncertainty in locating its band center. $2\nu_4$ exhibits the similar multiple Q branches of the fundamental. There is a certain internal consistency which arises, and indeed the lowest three combination bands predict that the unobserved lowest ν_{10} fundamental occurs between 125 and 135 cm^{-1}, a prediction that is not outrageous given the close agreement with the calculations and the estimate[24] from microwave spectroscopy but, nevertheless, disagreeing with the solution IR result of 297 cm^{-1}.[18]

Photoelectron Spectroscopy. The PE spectrum of **1** is shown in Figure 4 with experimental and calculated IPs given in Table 4. From a comparison with the known PE spectra of HCNO,[44] BrCNO,[7] NCCNO,[11] and ONCCNO[12] (see also ref 45), as well as from the calculated IPs, the assignment is relatively straightforward. In contrast to the PE spectra of the structurally different CH_3NCO[46,47] and CH_3OCN[2] molecules, that of **1** is consistent with C_{3v} symmetry. We note that both HAM/3 and OVGF give good agreement for the IPs, experiment and calculation agreeing within 0.6 eV. HAM/3 (hydrogenic atoms in molecules), which is known to give accurate representations of IPs of molecules containing first-row atoms,[48] is in particularly good agreement (within 0.3 eV). The OVGF calculations give a decided improvement over the Koopmans' values (Table 4). The sequence of molecular orbitals (MOs) deduced for **1** is

$$...(8a_1)^2(9a_1)^2(1e)^4(2e)^4(3e)^4$$

Molecular orbital plots are shown as insets in Figure 4. The observed PE spectrum up to 20 eV corresponds to five ionic states with the sequence X(^{2}E), A(^{2}E), B(^{2}E), C($^2A_1$), and D($^2A_1$). The first three bands at 9.92, 14.75, and 16.3 eV can, in the Koopmans' approximation, be assigned to the degenerate nonbonding π_{nb}(CNO), pseudo-π(CH_3), and bonding π_b(CNO) molecular orbitals, respectively. The first band at 9.92 eV has a narrow Franck−Condon profile in agreement with its assignment as a nonbonding orbital in a high-symmetry molecule, and is lower than those of the isomers CH_3NCO[46,47] (10.61 (a″) eV) and CH_3OCN[2] (11.30 (a″) eV). Notwithstanding the breaking of the degeneracy due to bending in CH_3NCO and CH_3OCN, the lower IP of **1** can be rationalized by the following simple orbital model; the π system of the −CNO, −NCO, or −OCN pseudohalide group is delocalized over the three atoms. The bonding orbitals (π_b) are delocalized over all three, whereas the nonbonding orbitals (π_{nb}) have a nodal plane at the central atom, perpendicular to the frame of the group. Thus, the π_{nb} orbital is localized on the two outer atoms, which for −NCO and −OCN are the two most electronegative (O and N), leading to a higher IP than in the case of −CNO. For comparison, the first IPs of the hydrogen derivatives HNCO[47] and HCNO[44] are 11.60 and 10.83 eV, respectively.

The second band in the PE spectrum at 14.75 eV with a broad Franck−Condon profile is assigned to the degenerate CH_3

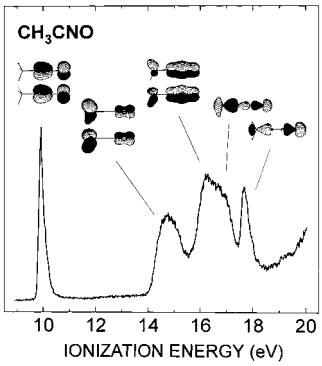

Figure 4. HeI photoelectron spectrum of CH_3CNO and schematics of the corresponding molecular orbitals.

TABLE 4: Experimental and Calculated Ionization Potentials (eV) of CH_3CNO

exptl IP[a]	HAM/3[b]	calcd OVGF[b]	KT[c]	orbital character
9.92	9.71 (e)	9.82	10.37	π_{nb}(CNO)
14.75	14.75 (e)	15.32	16.62	πCH_3
16.3	16.26 (e)	16.57	18.28	π_b(CNO)
17.0	16.77 (a_1)	16.84	18.59	σ(C−C)
17.68	17.98 (a_1)	18.02	19.82	$\sigma(n_O)$
	23.55 (a_1)	25.41	28.44	$\sigma(CH_3)$

[a] Vertical ionization potentials. [b] The B3-LYP/cc-pVTZ calculated geometry was used. [c] Koopmans' theorem IEs (HF//B3-LYP/cc-pVTZ).

TABLE 5: Calculated Geometries, Total and Relative Energies of $CH_3(CNO)$ Isomers, and Connecting Transition States[a]

no.	molecule[b] (1234)	type[b]	R_{12}	R_{23}	R_{34}	R_{24}[c] R_{14}[d]	α_{123}	α_{234}	α_{342},[c] α_{341}[d]	δ_{1234}	total energy (au), B3-LYP/6-31G **	rel energy (kcal/mol),[e] B3-LYP+ZPE	rel energy (kcal/mol)[e] CCSD(T)(full)// B3-LYP+ZPE
						Energy Minima							
3	CNCO	A	1.440	1.205	1.182		139.6	172.9		180.0	−207.991966	0	0
4	COCN	A	1.456	1.295	1.166		115.4	177.8		180.0	−207.944522	29.7	25.1
1	CCNO	A	1.460	1.165	1.218		180.0	180.0			−207.903433	54.9	57.4
5	CC(NO)	B	1.477	1.262	1.769	1.314	141.8	47.9	45.4	180.0	−207.877618	70.4	64.4
6	CONC	A	1.450	1.330	1.183		110.7	174.7		180.0	−207.854887	85.1	82.0
7	CN(OC)	B	1.468	1.563	1.291	1.439	109.7	59.7	69.6	105.2	−207.824792	102.8	97.8
						Transition States							
8	CCNO (5−3)	B	1.541	1.284	2.249	1.248	106.5	26.9	27.8	180.0	−207.849783	86.2	86.9
9	COCN (4−3)	C	2.126	1.262	1.201	2.491	63.5	176.3	49.0	180.0	−207.839871	92.9	91.6
10	CONC (6−4)	B	1.448	1.565	1.249	1.704	111.5	73.6	61.8	101.9	−207.811224	111.2	106.3
11	CN(OC) (7−)[f]	B	1.386	2.138	1.162	2.008	105.2	67.6	80.0	101.5	−207.803761	113.6	110.6
12	CCNO (5−1)	A	1.484	1.276	1.282		120.0	103.4		85.7	−207.802820	115.1	117.2
13	CNCO (7−1)	B	1.513	1.272	2.341	1.283	108.4	23.7	23.5	180.0	−207.783494	128.4	128.3
14	CONC (6−1)	C	2.451	1.244	1.208	2.774	75.6	166.9	62.3	0.0	−207.741824	153.5	150.9
15	CCNO (6−5)	C	1.926	1.253	1.435	1.981	117.2	83.1	105.3	0.0	−207.734376	158.2	153.7

[a] Geometries obtained at the B3LYP/6-31G** level. Bond lengths (R) are in Å, and bond angles (α) and dihedral angles (δ) are in deg. [b] See Figure 6 for the generalized shape of the structures and the text for explanations. The numbers in Figure 6 refer to the numbers in the table. [c] In the case of type B. [d] In the case of type C. [e] Energies relative to that of CH_3NCO. The 6-31G** basis set was used in the calculations. [f] Decomposition of **7** into CO and $H_2C{=}NH$.

pseudo-π orbital localized on the methyl group, which is mixed to some extent with π_b(CNO) (insets of Figure 4). Such CH_3 π orbitals typically occur between 14 and 16 eV in the analogous CH_3NCO and CH_3OCN molecules. The third band at 16.3 eV corresponds to the π_b(CNO) MOs and has a substantially broader Franck−Condon profile than that of π_{nb}(CNO), which reflects its assignment to the bonding CNO π orbitals. The third and fourth bands in the spectrum overlap, with the fourth observed as a shoulder at 17.0 eV. It originates from the highest lying σ orbital, which is delocalized over the whole CCNO frame, having a dominant contribution from the C−C bond (see the insets). The last observed band at 17.68 eV is assigned to the oxygen terminal lone pair orbital $n_O(8a_1)$, such an orbital giving rise to a sharp Franck−Condon profile in the spectra of HCNO[44] (17.79 eV), NCCNO[11] (18.75 eV), and BrCNO[7] (17.14 eV). No other bands are observed, in agreement with the calculations (Table 4) predicting the next IP in the inner valence region beyond the HeI (21.2 eV) range.

On the basis of the positive inductive effect (+I) of the CH_3 group, bands corresponding to the CNO group (π_{nb}(CNO), π_b-(CNO), and n_O) are expected to destabilize and shift toward lower IP compared to those of HCNO. Hence, the π_{nb}(CNO) orbital, which does not mix with the methyl group pseudo-π orbital, shifts from 10.83 eV in HCNO to 9.92 eV in **1**. The π_b(CNO) MOs, however, shift in the opposite direction (15.92 eV → 16.3 eV), demonstrating a substantial interaction between the methyl pseudo-π and CNO bonding π orbitals. This interaction overcompensates for the methyl group +I effect, thus stabilizing the π_b(CNO) orbitals.

Isomerization of 1. Figure 5 shows the calculated (B3-LYP/6-31G**) minima and linking TSs for isomerization processes in CH_3CNO (**1**), CH_3NCO (**3**), CH_3OCN (**4**), and CH_3ONC (**6**). The calculated total and relative energies (including the zero-point energy (ZPE)) of the minima and TSs are given in Table 5, with the structural labeling scheme presented in Figure 6. The present DFT calculations concur with the sequence of stabilities predicted previously using HF/STO-3G[25] and find two other minima, **5** and **7**, each being a methyl group attached to a three-membered ring, through either C (**5**) or N (**7**). Structure **5** is somewhat similar to both methyloxazirine and methylcarbonylnitrene, which the HF calculations identified as energetically close isomers with a small barrier between them, 11.0 and 23.8 kcal/mol from the nitrene and oxazirine sides, respectively. At the current higher level, these two minima have collapsed into **5**, which, from a comparison with typical C−N, C−O, and N−O single and double bonds,[49] has a C−N bond length akin to that of a double bond, a C−O between a single and double bond (49% double bond character), and an N−O much longer (ca. 0.32 Å) than a single bond. Such a structure for ring CH_3C-(NO), **5**, is in keeping with analogous structures calculated for HC(NO)[50,51] and NCC(NO).[52] The minimum-energy structure has a methyl CH eclipsing the CN bond, while the other possible conformer with methyl CH eclipsing the CO bond, noted

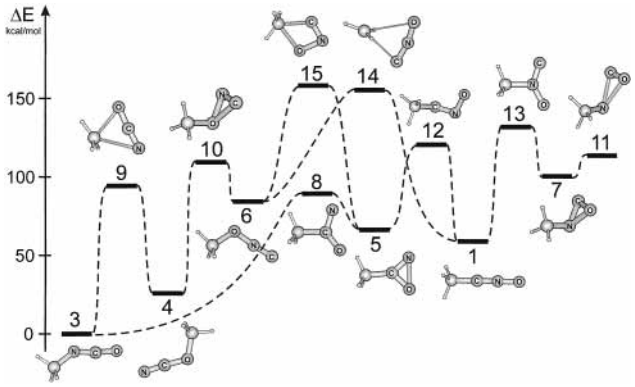

Figure 5. Calculated (B3-LYP/6-31G**) minima and transition states for isomerization processes for the four main open-chain isomers, CH_3-NCO, **3**, CH_3OCN, **4**, CH_3CNO, **1**, and CH_3ONC, **6**.

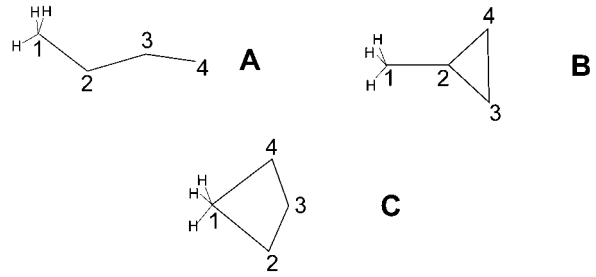

Figure 6. Structural configurations and labeling scheme for the calculated (B3-LYP/6-31G**) structures in Table 5.

previously,[25] is a TS corresponding to rotation of the CH_3 group around the C−C single bond. The other cyclic minimum, **7**, is energetically high lying, and was previously suggested[25] as an intermediate in the $H_3CONC \rightarrow H_3CNCO$ rearrangement. The present calculations show that **7** easily decomposes to CO and $H_2C{=}NH$ (via TS **11** and methylnitrene) with a small barrier of 12.8 kcal/mol (CCSD(T)//B3LYP + ZPE, Table 5). It can be regarded as a potential intermediate in the decomposition of **1** via the sequence **1** → **13** → **7** → **11** (Figure 5).

The room temperature stability of the methyl pseudohalides can be discussed in the context of the lowest energy path leading to isomerization. We apply here a well-known rule of thumb which states that a chemical reaction can proceed at room temperature if the barrier to the process is less than 20 kcal/mol. Molecules **1**, **3**, and **4** lie in deep wells on the potential energy surface (Figure 5), with the lowest isomerization barrier being 59.8, 86.9, and 66.5 kcal/mol, respectively. As far as intramolecular isomerization is concerned, the calculations confirm that these molecules are stable, consistent with the experimental observations of longevity in the dilute gas phase or in inert solid matrixes. **3** is a liquid at room temperature,[1] stable even in the condensed phase, and **4** can be cleanly generated in solid−gas reactions at room temperature, being semistable in the dilute gas phase.[2,3] **1** is observed in this work to be stable to isomerization in the gas phase and in the condensed phase at low temperatures.

Molecules **5** and **6** are in much shallower wells, with **5** isomerizing to **3** via TS **8** with a barrier of 22.5 kcal/mol, and **6** to **4** via TS **10** with a barrier of 24.3 kcal/mol, much less than the barrier of 43 kcal/mol suggested by the HF calculations, which also predicted an intermediate in a shallow well not found at the present level of theory. The barriers, however, are high enough to suggest that spectroscopic investigation of **5** and **6** may be feasible at room temperature or lower, although they can isomerize at higher temperatures. As far as we know **5** has not been identified, but **6** has, as a minor component among the cold (−196 °C) trapped reaction products of the FVP of 3-methyl-4-(*O*-methyloximino)isoxazol-5(4*H*)-one,[4] with the suggested intramolecular decomposition process being that predicted here. Molecule **7**, as discussed above, is not stable at room temperature.

The geometries of the TSs (Figure 5, Table 5) clearly represent the structural changes that the molecules make during the isomerization processes. The pseudohalide "normal" ↔ "iso" (viz., cyanate **4** ↔ isocyanate **3**, and fulminate **6** ↔ isofulminate (nitrile oxide) **1**) rearrangements proceed via four-membered planar rings (structures **9** and **14**), where the methyl group is simply transferred from one end of the pseudohalide frame to the other. The barrier for these processes is high, 66.5 and 68.9 kcal/mol for **4** → **3** and **6** → **1**, respectively, the latter having been previously calculated at the HF/STO-3G level[25] (66 kcal/mol), in good agreement with the present results. The well-known condensed-phase cyanate → isocyanate rearrangement at room temperature cannot be explained by intramolecular isomerization processes, and so bi- or polymolecular reactions may be involved.

The type of isomerization where the pseudohalide group bends strongly to form a three-membered ring which consecutively opens up to form another isomer has been discussed above. We note here that this is a typical process in the normal ↔ normal (fulminate **6** ↔ cyanate **4**) and iso ↔ iso (isofulminate **1** ↔ isocyanate **3**) isomerization processes with barriers (**6** → **4**, 24.3 kcal/mol; **1** → (**5**) → **3**, 59.8 kcal/mol) smaller than those of the corresponding normal → iso rearrangements with barriers for **6** → **1** and **1** → **6** of 68.9 and 93.5 kcal/mol and for **4** → **3** and **3** → **4** of 66.5 and 91.6 kcal/mol. This type of isomerization can proceed without, e.g., **6** → **4**, or with the intermediacy of a non-pseudohalide intermediate (**1** → (**5**) → **3**). The latter is a standard loss process for large nitrile oxides to isocyanates at elevated temperatures,[5] and was proposed as a potential loss route for photochemically induced RCNO → RNCO rearrangements in low-temperature matrixes.[53] For **1** at room temperature, however, this is not favored, the alternative loss route for such small nitrile oxides being intermolecular dimerization, a much lower energy process.

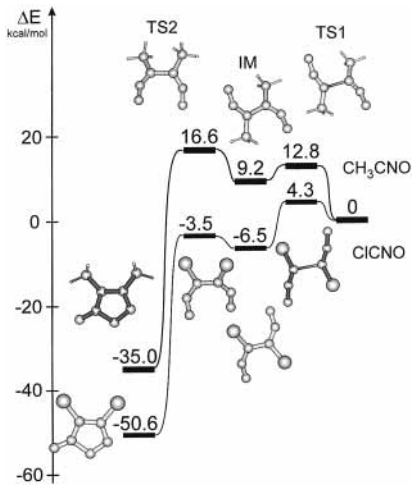

Figure 7. Calculated (B3-LYP/6-31G**) least energy surface for the dimerization of CH_3CNO to the ring furoxan, and comparison with the corresponding dimerization process for ClCNO.

Dimerization of Acetonitrile *N*-Oxide, 1, to Dimethylfuroxan, 2. The short lifetime of **1**, and indeed other small nitrile oxides, has been long known to be due to dimerization to the furoxan, with presumed low activation barriers. Such dimerizations are a special type of [3+2] dipolar cycloaddition, where both the 1,3- and the 1,2-dipoles are nitrile oxides. We have calculated this surface for **1** at the B3-LYP/6-31G** level following a procedure similar to that used for the dimerization of ClCNO.[9] Mechanisms for such 1,3-dipolar cycloaddition reactions have engendered considerable discussion because a definitive choice between the two main mechanisms could not be made (see, for example, ref 54), the issues relating to a simultaneous one-step process,[55,56] or a sequential two-step mechanism[57] in which only one σ bond forms in the first step.

Figure 7 shows the lowest energy reaction path on the potential surface for this process, comparing it to that for the ClCNO case. A Firestone-type process is indicated, a two-step mechanism, where the first step proceeds via **TS1** with an energy barrier of 12.8 kcal/mol, where the two dipoles are in an extended conformation (NCCN dihedral angle, 180°; C−C bond length, 1.875 Å) to an intermediate (**IM**) with a close to planar (NCCN dihedral angle, 150°) structure and a shorter CC bond (1.550 Å). This may be identified as the Firestone intermediate. In the second step the extended intermediate **IM** closes with rotation around the established C−C single bond to the final five-membered furoxan ring **2** after passing over **TS2** with an energy barrier of 7.4 kcal/mol. Since **TS2** is higher in energy than **TS1**, the second step is rate determining. The overall barrier of 16.6 kcal/mol at **TS2** compared to the energy of two monomers is relatively low, predicting that dimerization of **1** must be rapid at room temperature, but high enough to prevent dimerization at lower temperatures. This concurs with our experimental observation (PE and IR spectra) that **1** can be

isolated at low temperatures and revaporized below 0 °C without significant loss to the dimer. As Figure 7 illustrates, the dimerization mechanisms of **1** and ClCNO[9] are very similar, following a two-step process, but with significantly different barriers. That for ClCNO is a mere 4.3 kcal/mol, indicative of a process that can go to completion very easily, thereby explaining the spontaneous and rapid dimerization of ClCNO observed experimentally at room temperature.

Conclusion

In this work we have sought to generate CH_3CNO, **1**, cleanly in the gas phase for spectroscopic observation, to compare structural and spectroscopic data with conventional ab initio methods and DFT methods, and to describe, computationally, potential loss processes via either isomerization or dimerization pathways. The method chosen, thermolytic cycloreversion of the ring dimer dimethylfuroxan, **2**, turns out to be an excellent approach permitting the acquisition of clean gas-phase photoionization mass, mid-infrared, and HeI photoelectron spectra. The gas-phase IR spectrum, assigned on the basis of band shapes and a comparison with computational results, provides a clear picture of a symmetric-top molecule and should provide a useful starting point for high-resolution investigation.[58] The HeI photoelectron spectrum was assigned on the basis of C_{3v} symmetry and is in excellent agreement with both HAM/3 and OVGF calculations for the ionization energies. The structure investigated with medium- to large-scale ab initio calculations demonstrates the continued difficulty for conventional ab initio calculations due to strong correlation effects. Nonetheless, DFT can be a cost-effective approach for such molecules, and this approach was used to investigate differences in the potential surfaces of **1**, CH_3NCO, and CH_3OCN reflective of their structural differences, and isomerization processes to chain and ring species. The conclusion is that **1** has a linear or quasi-linear heavy atom chain and is stable to unimolecular decomposition, and as demonstrated by DFT calculations, dimerization to the stable furoxan is the dominant loss process involving a two-step mechanism. Nonetheless, loss through dimerization is shown to be not as significant as in the case of the halosubstituted nitrile oxide ClCNO and, by extension, BrCNO.

Acknowledgment. We thank the Hungarian Scientific Research Fund (OTKA Grant F022031) and the Natural Sciences and Engineering Research Council of Canada (NSERC) for research and equipment grants in support of this work. T.P. thanks the Hungarian Academy of Sciences for the award of a Janos Bolyai research scholarship.

References and Notes

(1) Kricheldorf, R.; Leppert, E. *Synthesis* **1976**, 329.

(2) Pasinszki, T.; Westwood, N. P. C. *J. Phys. Chem.* **1995**, *99*, 1649.

(3) Sakaizumi, T.; Mure, H.; Ohashi, O.; Yamaguchi, I. *J. Mol. Spectrosc.* **1990**, *140*, 62. Sakaizumi, T.; Sekishita, K.; Furuya, K.; Tetsuda, Y.; Kaneko, K.; Ohashi, O.; Yamaguchi, I. *J. Mol. Spectrosc.* **1993**, *161*, 114. Sakaizumi, T.; Namikawa, M.; Ohashi, O. *J. Mol. Struct.* **1995**, *345*, 189.

(4) Wentrup, C.; Gerecht, B.; Laqua, D.; Briehl, H.; Winter, H.-W.; Reisenauer, H. P.; Winnewisser, M. *J. Org. Chem.* **1981**, *46*, 1046. The choice of nomenclature for compounds of the type RONC is variable. As noted in this reference, and as used in the present paper, we use the IUPAC name "fulminate" for RONC (NOC rule C-833.1; GNOC recommendation R-5.9.7.2).

(5) Grundmann, Ch.; Grunanger, P. *The Nitrile Oxides, Versatile Tools of Theoretical and Preparative Chemistry*; Springer-Verlag: New York, Heidelberg, Berlin, 1971. Torssell, K. B. G. In *Nitrile Oxides, Nitrones, and Nitronates in Organic Synthesis*; Feuer, H., Ed.; Organic Nitro Chemistry Series; VCH Publishers Inc.: New York, 1988.

(6) Diana, G. D.; Cutcliffe, D.; Volkots, D. L.; Mallamo, J. P.; Bailey, T. R.; Vescio, N.; Oglesby, R. C.; Nitz, T. J.; Wetzel, J.; Giranda, V.; Pevear, D. C.; Dutko, F. J. *J. Med. Chem.* **1993**, *36*, 3240. Amici, M. De; Micheli, C. De; Misani, V. *Tetrahedron* **1990**, *46*, 1975.

(7) Pasinszki, T.; Westwood, N. P. C. *J. Phys. Chem.* **1995**, *99*, 6401.

(8) Gillies, C. W.; Gillies, J. Z.; Lichau, H.; Winnewisser, B. P.; Winnewisser, M. *Chem. Phys. Lett.* **1998**, *285*, 391.

(9) Pasinszki, T.; Westwood, N. P. C. *J. Phys. Chem. A* **1998**, *102*, 4939.

(10) Lichau, H.; Winnewisser, B. P.; Winnewisser, M.; Gillies, C. W.; Gillies, J. Z. To be published.

(11) Pasinszki, T.; Westwood, N. P. C. *J. Phys. Chem.* **1996**, *100*, 16856.

(12) Pasinszki, T.; Westwood, N. P. C. *J. Am. Chem. Soc.* **1995**, *117*, 8425.

(13) Guo, B.; Pasinszki, T.; Westwood, N. P. C.; Bernath, P. F. *J. Chem. Phys.* **1995**, *103*, 3335.

(14) Guo, B.; Pasinszki, T.; Westwood, N. P. C.; Zhang, K.-Q.; Bernath, P. F. *J. Chem. Phys.* **1996**, *105*, 4457.

(15) Brupbacher, Th.; Bohn, R. K.; Jäger, W.; Gerry, M. C. L.; Pasinszki, T.; Westwood, N. P. C. *J. Mol. Spectrosc.* **1997**, *181*, 316.

(16) Koput, J. *J. Phys. Chem. A* **1999**, *103*, 2170.

(17) Koput, J. *J. Phys. Chem. A* **1999**, *103*, 6017.

(18) Isner, W. G.; Humphrey, G. L. *J. Am. Chem. Soc.* **1967**, *89*, 6442.

(19) Zinner, G.; Günther, H. *Angew. Chem., Int. Ed. Engl.* **1964**, *3*, 383.

(20) Mitchell, W. R.; Paton, R. M. *Tetrahedron Lett.* **1979**, *26*, 2443.

(21) Mielke, Z.; Hawkins, M.; Andrews, L. *J. Phys. Chem.* **1989**, *93*, 558.

(22) Bodenseh, H. K.; Morgenstern, K. *Z. Naturforsch.* **1970**, *25a*, 150.

(23) Blackburn, P. B.; Brown, R. D.; Burden, F. R.; Crofts, J. G.; Gillard, I. R. *Chem. Phys. Lett.* **1970**, *7*, 102.

(24) Winnewisser, M.; Pearson, E. F.; Galica, J.; Winnewisser, B. P. *J. Mol. Spectrosc.* **1982**, *91*, 255. Galica, J.; Winnewisser, M.; Winnewisser, B. P. *J. Mol. Struct.* **1984**, *114*, 243.

(25) Poppinger, D.; Radom L. *J. Am. Chem. Soc.* **1978**, *100*, 3674.

(26) Wiberg, K. B.; Breneman, C. M. *J. Am. Chem. Soc.* **1990**, *112*, 8765.

(27) Koput, J.; Winnewisser, B. P.; Winnewisser, M. *Chem. Phys. Lett.* **1996**, *255*, 357.

(28) Scholl, *Chem. Ber.* **1890**, *23*, 3499.

(29) Ungnade, H. E.; Kissinger, L. W. *Tetrahedron* **1963**, *19* (Suppl. 1), 143.

(30) Frost, D. C.; S. T. Lee, S. T.; McDowell, C. A.; Westwood, N. P. C. *J. Electron Spectrosc. Relat. Phenom.* **1977**, *12*, 95.

(31) Pasinszki, T.; Westwood, N. P. C. *J. Mol. Struct.* **1997**, *408/409*, 161.

(32) Åsbrink, L.; Fridh, C.; Lindholm, E. *Chem. Phys. Lett.* **1977**, *52*, 69. The HAM/3 program (PC version) is available from the QCPE, Indiana University, Bloomington, IN (Chong, D. P. QCMP005, 1985).

(33) Niessen, W. von; Schirmer, J.; Cederbaum, L. S. *Comput. Phys. Rep.* **1984**, *1*, 57.

(34) Frisch, M. J.; Trucks, G. W.; Head-Gordon, M.; Gill, P. M. W.; Wong, M. W.; Foresman, J. B.; Johnson, B. G.; Schlegel, H. B.; Robb, M. A.; Replogle, E. S.; Gomperts, R.; Andres, J. L.; Raghavachari, K.; Binkley, J. S.; Gonzalez, C.; Martin, R. L.; Fox, D. J.; Defrees, D. J.; Baker, J.; Stewart, J. J. P.; Pople, J. A. Gaussian 92, Revision E.1, Gaussian, Inc., Pittsburgh, PA, 1992.

(35) Frisch, M. J.; Trucks, G. W.; Schlegel, H. B.; Gill, P. M. W.; Johnson, B. G.; Robb, M. A.; Cheeseman, J. R.; Keith, T. A.; Petersson, G. A.; Montgomery, J. A.; Raghavachari, K.; Al-Laham, M. A.; Zakrzewski, V. G.; Ortiz, J. V.; Foresman, J. B.; Cioslowski, J.; Stefanov, B. B.; Nanayakkara, A.; Challacombe, M.; Peng, C. Y.; Ayala, P. Y.; Chen, W.; Wong, M. W.; Andres, J. L.; Replogle, E. S.; Gomperts, R.; Martin, R. L.; Fox, D. J.; Binkley, J. S.; Defrees, D. J.; Baker, J.; Stewart, J. P.; Head-Gordon, M.; Gonzalez, C. and Pople, J. A.: Gaussian 94, Revision D.4, Gaussian, Inc., Pittsburgh, PA, 1995.

(36) Flammang, R.; Barbieux-Flammang, M.; Gerbaux, P.; Wentrup, C.; Wong, M. W. *Bull. Soc. Chim. Belg.* **1997**, *106*, 545.

(37) Pople, J. A.; Head-Gordon, M.; Raghavachari, K. *Int. J. Quantum Chem., Quantum Chem. Symp.* **1988**, *22*, 377. Kraka, E.; Gauss, J.; Cremer, D. *J. Mol. Struct.*: *THEOCHEM* **1991**, *80*, 95.

(38) He, Z.; Cremer, D. *Int. J. Quantum Chem., Quantum Chem. Symp.* **1991**, *25*, 43. He, Z.; Cremer, D. *Theor. Chim. Acta* **1993**, *85*, 305.

(39) Calculated equilibrium geometry for CH_3NCO using B3-LYP/cc-pVTZ and experimental MW (r_0) results (Koput, J. *J. Mol. Spectrosc.* **1986**, *115*, 131) in parentheses: C—N = 1.439 (1.4507) Å, N═C = 1.197 (1.214) Å, C═O = 1.173 (1.166) Å, C—N—C = 139.9° (135.6°), N—C—O = 173.7° (170.3°).

(40) Calculated equilibrium geometry for CH_3OCN using B3-LYP/cc-pVTZ and experimental MW (r_s) results (ref 3) in parentheses: C—O = 1.456 (1.455) Å, O—C = 1.287 (1.302) Å, C≡N = 1.156 (1.146) Å, C—O—C = 115.6° (113.8°), O—C—N = 177.9° (178.4°).

(41) Pasinszki, T.; Westwood, N. P. C. To be published.

(42) Teller, E. *Hand-und Jahrb. d. Chem. Phys.* **1934**, *9* (*II*), 43.

(43) Parker, F. W.; Nielsen, A. H.; Fletcher, *J. Mol. Spectrosc.* **1957**, *1*, 107. Nakagawa, I.; Shimanouchi, T. *Spectrochim. Acta, A* **1962**, *18*, 513.
(44) Bastide, J.; Maier, J. P. *Chem. Phys.* **1976**, *12*, 177.
(45) Pasinszki, T.; Westwood, N. P. C. *J. Electron Spectrosc. Relat. Phenom.* **1998**, *97*, 15.
(46) Cradock, S.; Ebsworth, E. A. V.; Murdoch, J. D. *J. Chem. Soc., Faraday Trans. 2* **1972**, *68*, 86. Pasinszki, T.; Yamakado,; H.; Ohno, K. *J. Phys. Chem.* **1993**, *97*, 12718.
(47) Eland, J. D. H. *Philos. Trans. R. Soc. London, A* **1970**, *268*, 87.
(48) Chong, D. P. *Theor. Chim. Acta* **1979**, *51*, 55.
(49) Calculated CN, CO, and NO bond lengths in $H_2C{=}NH$, $H_3C{-}NH_2$, $H_2C{=}O$, $H_3C{-}OH$, and $H_2N{-}OH$ at the B3LYP/6-31G** level are 1.270, 1.464, 1.207, 1.418, and 1.448 Å, respectively.
(50) Mebel, A. M.; Luna, A.; Lin, M. C.; Morokuma, K. *J. Chem. Phys.* **1996**, *105*, 6439.
(51) Jursic, B. S.. *J. Phys. Chem. A* **1999**, *103*, 1880.
(52) Fehér, M.; Pasinszki, T.; Veszprémi, T. *Inorg. Chem.* **1995**, *34*, 945.
(53) Maier, G.; Teles, J. H. *Angew. Chem., Int. Ed. Engl.* **1987**, *26*, 155.
(54) Houk, K. N.; Yamaguchi, K. In *1,3-Dipolar Cycloaddition Chemistry*; Padwa, A., Ed.; Wiley-Interscience: New York, 1984; Vol. 2.
(55) Huisgen, R. *Angew. Chem., Int. Ed. Engl.* **1963**, *2*, 565; *J. Org. Chem.* **1968**, *33*, 2291; **1976**, *41*, 403.
(56) Huisgen, R. In *1,3-Dipolar Cycloaddition Chemistry*; Padwa, A., Ed.; Wiley-Interscience: New York, 1984; Vol. 1.
(57) Firestone, R. A. *J. Org. Chem.* **1968**, *33*, 2285; **1972**, *37*, 2181; *J. Chem. Soc. A* **1970**, 1570; *Tetrahedron* **1977**, *33*, 3009.
(58) B. P. Winnewisser and M. Winnewisser have indicated (private communication to N.P.C.W.) that they have some unpublished high-resolution IR data on **1**.